Tuneable Multicoloured Patterns From Photonic Cross Communication Between Cholesteric Liquid Crystal Droplets†

JungHyun Noh,[a] Hsin-Ling Liang,[b] Irena Drevensek-Olenik,[c] and Jan P. F. Lagerwall*[a]

Received Xth XXXXXXXXXX 20XX, Accepted Xth XXXXXXXXX 20XX
First published on the web Xth XXXXXXXXXX 200X
DOI: 10.1039/b000000x

Monodisperse droplets of planar-aligned cholesteric (N*) liquid crystal exhibit an intriguing capacity for photonic cross communication, giving rise to colourful patterns that depend sensitively on N* pitch, droplet positions and illuminated area. The phenomenon results from a combination of omnidirectional selective reflection of N* droplets—which thus act as spherically symmetric self-assembled photonic crystals—and total internal reflection at the continuous phase surface. We outline how the unique optical properties can be employed in numerous applications.

Cholesteric liquid crystals are recognised as extraordinary soft photonic materials, providing UV, visible or IR selective (Bragg) reflection at wavelengths that are easily tuned by chemical composition, temperature or confinement[1–5] and that can be utilised in numerous applications, including sensors[6,7] and tuneable lasers.[8–10] Moreover, since the self-assembled periodic structure that is at the heart of this photonic crystal behaviour is helical, the reflected light is circularly polarised with the same handedness as the helix of the cholesteric phase (N*).[1] Traditionally cholesterics have been used in flat sample geometries, e.g. for devices like temperature[11] or gas sensors.[12] Today there is a rapidly growing interest in drops or shells of liquid crystal,[13,13–21] as the spherical topology gives rise to peculiar phenomena[22] and application potential in e.g. actuators[23] or lasers.[9,24] In this *Communication* we demonstrate a new attractive property of N* droplets that are sufficiently monodisperse to form hexagonally close-packed colloidal crystal arrangements. Multiple modes of photonic communication between droplets develop, giving rise to feature-rich and multicoloured patterns. The details can be tuned either by acting on the cholesteric (changing the pitch p of its helix) or on the continuous phase that surrounds the droplets, or by changing the size of the illuminated area. We describe and explain the phenomenon and outline how the dynamic and sensitive set of patterns could be applied in e.g. all-optical communication switches, light couplers, sensors or high-security identification/anti-counterfeiting tags.

A microfluidic set-up is used to produce monodisperse N* droplets at high throughput in an aqueous continuous phase (see ESI† for details). The droplet diameter is on the order of 100 μm and the helix orientation is almost uniformly radial, as confirmed by the appearance of a central spot with the colour of normal-incidence selective reflection of the cholesteric mixture (see ESI Fig. 1-2)†. In a hexagonally close-packed arrangement of droplets, an additional regular arrangement of spots with other colours appears if p is fairly long, e.g. as in the fundamentally red-reflecting droplets in Fig. 1 and in pane (c) of ESI Fig. 1†. The spots make up patterns with the same hexagonal symmetry as the large-scale colloidal crystal.

We investigated these patterns in detail with relatively large droplets of an N* mixture with fundamental reflection at $\lambda_r^{air} = 646$ nm, corresponding to $p \approx 430$ nm (this follows from an average refractive index $n_{av} \approx 1.5$ for the mixture[5]). Smaller droplets yield analogous results, as shown in ESI Fig. 3†, but they are more difficult to collect in a regular colloidal crystal arrangement within the liquid continuous phase (present in large excess) and the smaller scale of the optical patterns makes the analysis less accurate. The results are summarised in Fig. 1, showing the development as the illuminated area is gradually expanded. Initially the field aperture of the microscope is set to its minimum, such that the illumination spot is less than the cross section of a single droplet. This droplet then shows only a central selective reflection spot with the fundamental red colour (a). Interestingly, we also see a hexagonal pattern of twelve spots in the *surrounding* droplets, an inner ring of blue spots and an outer ring of green-yellow spots. Since only the central droplet is illuminated we conclude that these spots must arise as a result of light being reflected horizontally from the central droplet into the surrounding droplets, which reflect it back up to the objective.

† Electronic Supplementary Information (ESI) available: [Experimental details and complementary experiments]. See DOI: 10.1039/b000000x/

[a] *Graduate School of Convergence Science & Technology and Advanced Institutes of Convergence Technologies, Seoul National University, Suwon-si, Gyeonggi-do, Korea 443-270.*
Tel: +82 (0)31 888 9165; E-mail: jan.lagerwall@lcsoftmatter.com
[b] *Institute of Organic Chemistry, Johannes Gutenberg University Mainz, Duesbergweg 10-14, 55099 Mainz, Germany.*
[c] *University of Ljubljana, Faculty of Mathematics and Physics, Jadranska 19, SI 1000 Ljubljana, Slovenia and J. Stefan Institute, Jamova 39, SI 1000 Ljubljana, Slovenia.*

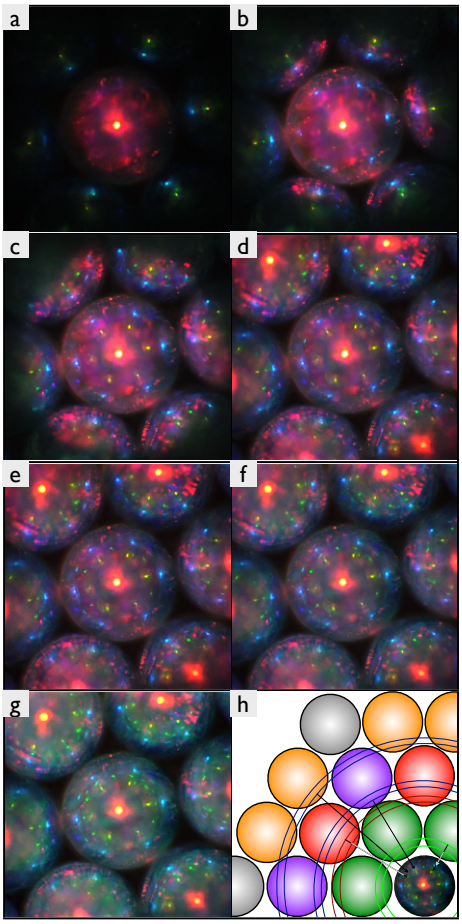

Fig. 1 A hexagonally close-packed array of droplets of a red-reflecting cholesteric, observed in reflection between crossed polarisers as the field diaphragm is continuously opened (a-g). Higher-order reflections are blurred and some spots are missing from the complete pattern, reflecting the greater disturbance in long-distance photonic communication. (h) Schematic of the inter-droplet photonic communication giving rise to the patterns.

When the field aperture is opened enough for the illuminated area to reach the blue spots seen from the beginning in the surrounding droplets, the same blue spots appear, with six-fold symmetry, also in the central droplet (Fig. 1b). The distance from the perimeter is identical to the corresponding distance for the blue spots in the surrounding droplets. The symmetry clearly indicates the cross communication between the droplets. A further opening of the aperture until also the range of green-yellow spots in the surrounding droplets is illuminated leads to the appearance of identical spots in the central droplet (Fig. 1c). The hexagonal spot pattern matches the arrangement of nearest neighbour (*nn*) droplets, as it has to if they arise from reflections between these droplets.

As we continue to open the aperture, first the fundamental red spot appears also at the centre of each surrounding droplet, next yet another hexagonal set of blue spots appears in the central droplet, cf. Fig. 1d. These spots, offset with respect to *nn* droplets by 30°, are followed by a new set of green spots, further inside, with the same azimuthal arrangement (Fig. 1e). The locations of these two sets of second-generation spots, and the fact that they appear once the illumination area extends outside the pictured area in Fig. 1, indicates that they arise through photonic communication between next nearest neighbour (*nnn*) droplets. Patterns from next next nearest neighbour (*nnnn*) and next next next nearest neighbour (*nnnnn*) photonic communication follow in panes (f) and (g), respectively, before the aperture is fully open. In pane (h) we have summarised the observations in a schematic that depicts the central droplet, as it appears under fully opened field aperture, together with cartoon droplets surrounding it in the upper left-hand quadrant. The series of spots originate from the same two types of reflection, from successively more distant neighbour droplets. This is illustrated with a sequence of concentric rings indicating the boundary of the illuminated area each time a new set of spots appears in the central droplet, together with a representative arrow from each ring to a corresponding reflection spot.

We refer to the schematic in Fig. 2 for explaining the observations. The central red spot corresponds to normal incidence selective reflection, indicated by the double arrow labeled (0). The first set of peripheral spots appears when the illumination beam (1) meets the cholesteric neighbour droplets at an angle of incidence $\theta = 45°$. The droplets reflect the light from vertical to horizontal, particularly in the wavelength regime that fulfils the Bragg condition for the N* helix at this θ-value. Moreover, the helix-reflected light gets circularly polarised, such that it is reflected with little loss by the next droplet in its path (the central droplet) back into the vertical direction. The circular polarisation ensures that the light goes through the analyser to 50% and we can thus clearly see the spot despite crossed polarisers. The Bragg condition (Fig. ESI2)[†] is fulfilled when the light wavelength in the liquid crystal $\lambda_{LC} = p\cos\theta$ which for p =430 nm and $\theta = 45°$ yields $\lambda_{LC} = 304$ nm. With $n_{av} = 1.5$ this translates into an air wavelength λ_{air}=456 nm, matching the observed blue colour of the spots corresponding to this direct (*D*) inter-droplet communication.

The next spots appear when the illuminated area has grown to encompass ray (2). Because it is closer to the centre of the neighbour droplet this ray meets the cholesteric at an angle α that is smaller than 45°. Fulfilling the Bragg condition thus requires a greater wavelength $\lambda_{LC} = p\cos\alpha$. The reflected beam is directed towards the surface of the continuous phase, where it will be totally internally reflected (*TIR*) because of the greater refractive index compared to the external air phase. As illustrated in Fig. 2 there is a specific value of α that will place

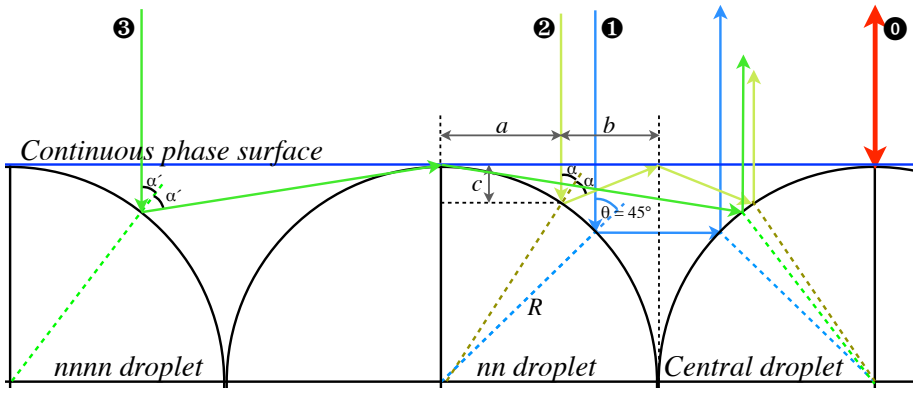

Fig. 2 Schematic of direct (*D*) photonic communication between nearest neighbour (*nn*) droplets giving rise to the blue spots in Fig. 1, and of the communication path mediated via total internal reflection (*TIR*) against the surface of the continuous phase, here illustrated for the case of *nn* and next next nearest neighbour (*nnnn*) droplets.

the reflection point exactly mid point between the two adjacent droplets, and by symmetry the *TIR* beam will then enter the centre droplet at the same angle α, meaning that the same wavelength will be Bragg-reflected up into the vertical direction, going through the objective and to the observer. This is the origin of the green-yellow spots. The triangle formed by the original downwards-directed beam (2), the first selectively reflected beam and the surface of the continuous phase (see Fig. 2 for definitions of the distances), gives that

$$\tan 2\alpha = b/c = \frac{R - R\sin\alpha}{R - R\cos\alpha} = \frac{1-\sin\alpha}{1-\cos\alpha} \qquad (1)$$

which we solve graphically, obtaining $\alpha \approx 34°$. Through $\lambda_{air} = n_{av} p \cos\alpha$, with p =420 nm and $n_{av} \approx 1.5$, this gives us selective reflection at approximately 535 nm, fitting with the observed green-yellow spot colour.

With expanding illumination the same sequence of direct (*D*) and *TIR*-mediated inter-droplet communication takes place involving the *nnn* droplets. As seen in Fig. 1h this occurs in a different plane than that of Fig. 2, hence it is not drawn there. The next case drawn is instead the *nnnnTIR* communication beginning with ray (3). For growing illuminated area new cases of longer-range *TIR*-mediated communication become possible, but direct (*D*) communication is absent beyond the *nnn* case since it is prevented by the intermediate droplets.

For both cases of *D* communication the reflection conditions are the same since the ray direction between droplets is horizontal. All *D* spots thus have the same blue colour and they all appear at the same distance from the droplet centre. In contrast, the spots occurring as a result of *TIR* at the top surface involve droplet reflection at an angle α, α'... that grows with increasing inter-droplet separation (see Fig. 2). The reflected wavelength then decreases, blue-shifting the spots from longer communication paths. Comparing the second set of *nn* spots with the second set of *nnn* spots we see that the latter is indeed greenish while the former is yellow. The *nnnnn* spots in pane (g) are blueish.

To corroborate that all peripheral spots inside the outermost ring indeed arise from ray paths that include a *TIR* event at the top surface we conducted an experiment where we added continuous phase and followed the reflection pattern, cf. Fig. ESI4 and Movie ESI6 and related text in the ESI.[†] As expected, the increased distance to the surface red-shifts the spots and places them closer to the perimeter. We also measured the reflection spectrum from one set of droplets, cf. Fig. ESI5 and related discussion. This essentially confirmed the model described above but the quantitative data show that the helix axis is in fact inclined by a slightly larger angle than expected, 45.9°. As explained in the ESI this is most likely a result of a slight droplet flattening resulting from the competition between buoyancy (driving droplets upwards) and surface tension of the continuous phase (pushing them downwards).

A simple way of tuning the pattern is to vary the cholesteric helix pitch. If we increase p to 545 nm we get normal incidence selective reflection at $545 \cdot 1.5 = 818$ nm, i.e. in the IR range. No central spot will then be visible but the outer row of peripheral spots is still in the visible spectrum, as its reflection wavelength is given by $\lambda_{air} = 1.5 p \cos 45° = 578$ nm. For the *nn-TIR* spots in the inner peripheral row the reflection wavelength is $1.5 p \cos 34° = 678$ nm which is on the border of being detectable visibly. We prepared droplets with such an increased pitch and conducted the same experiment as in Fig. 1, confirming the calculated data, cf. Fig. 3a. Neither the central spot nor the *nn-TIR* spots can be seen, but the *D* spots are clearly visible, now with an orange-red colour. Increasing the amount of chiral dopant in the mixture gradually, we decrease p and thereby blue-shift the reflection colours step by step, as demonstrated in panels b-f. When p is down to

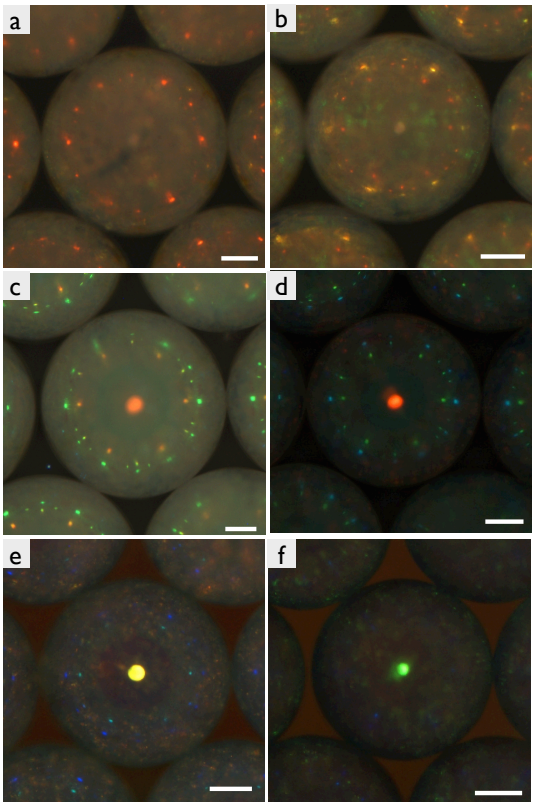

Fig. 3 Reflection pattern in the central droplet and its immediate surrounding in colloidal crystals of cholesteric droplets with decreasing pitch, from long enough to give only infrared normal reflection in (a) to green-reflecting at normal incidence in (f). Scale bars are 100 μm.

360 nm the central spot has a yellow-green colour at about 540 nm wavelength and only the *nn-TIR* peripheral spots are detectable with a deep violet colour. The *D* spots are now in the UV range and thus invisible.

The peculiar optical properties of this colloidal crystal of N* droplets, and the sensitivity of the pattern to helix pitch, illuminated area and droplet positions, open multiple paths to device application. In fact, the elucidation of the patterns implies that already an isolated droplet behaves very interesting. Under white light from above it functions like an unusual spectrometer, separating the incident ray into cones of light with different wavelengths. For the cone with 180° opening angle (giving rise to *D* reflections when adjacent droplets are present) light is distributed uniformly within a well defined plane. If a second identical droplet is added it will reflect this light back up into the vertical direction, regardless of its location (this is illustrated in ESI Fig. 3†). The location of the spot on that droplet points to where the original droplet is.

The system of hexagonally close-packed droplets combines the functions of a retroreflector, translating the reflected beams laterally in a highly regular pattern, with a monochromator, each spot having a well-defined narrow wavelength span. Moreover, the two types of inter-droplet communication (*D* and *TIR*-mediated) provide two independent means of tuning the wavelengths. All spots shift in colour if *p* is changed (e.g. by heating or cooling a temperature sensitive mixture or—as done above—by changing the composition), but if *p* is kept constant while the droplet–surface distance is changed the *TIR* spots are wavelength-shifted and moved while the *D* spots are unaffected. As the reflected light additionally is circularly polarised we have a system with truly unique and tuneable optical properties that are very difficult—if not impossible—to reproduce by other means. This constitutes a beautiful example of the advanced functional systems that the different modes of self-assembly in ordered soft matter can give rise to.

By using reactive mesogens the droplets can be polymerised in order to make the cholesteric structure permanent,[25] and/or the continuous phase can be polymerised, into a rubber[26] or into a glass.[27] A rubbery or solid phase surrounding liquid crystalline droplets can be most attractive as a device can then easily be handled and integrated into larger systems, while the full tuneability related to N* helix modulation is retained. To give a taste of what could be achieved we here outline four potential applications of cholesteric droplets, taking advantage of their unusual optical properties.

- The simplest application, requiring only a single droplet, would take advantage of the fact that light with the wavelength of the *D* spots described above is reflected into a plane perpendicular to the incident beam, into all directions within this plane. This turns a cholesteric droplet into an ideal optical coupler for cases when a flat sample needs to be illuminated uniformly, e.g. in microfluidic chips or flat liquid crystal devices. Since the wavelength that is coupled into the plane is easily tuned via *p*, this wavelength can either be modulated dynamically, or different types of droplets can be introduced into the sample, with different compositions producing different helix pitches, thus coupling different wavelengths into the plane. For instance, by introducing three droplet types, optimised for coupling, red, green and blue light, respectively, any colour can be coupled into the plane by illuminating the three droplet types with varying intensities.

- An all-optical distributor/switch could be realised from hexagonally close-packed droplets, where a single input is routed to different sets of regularly spaced outputs. By changing the input wavelength different outputs are activated or the output can be turned off completely. Since the origin of the wavelength selectivity is structural and since *p* is tuneable from infinity to the UV range such a device can be designed (and dynamically redesigned) to operate at any wavelength that is not absorbed too

strongly by the materials involved, including the infrared regime for optical data transmission.

- A third application route is in autonomous sensors. The system's softness and the sensitivity to p and to the droplet positions renders the system an excellent basis for sensors of pressure, tension, temperature and various other parameters, with an optical read-out and without any power consumption. Either the droplets or the continuous phase (or both) should be polymerised in order to achieve a material that is convenient to handle.

- Finally, the uniqueness of the reflection pattern provides an excellent base for realising high-security identification tags. Because the reflected light is circularly polarised, because it may include the invisible UV and/or IR ranges, and because the number, wavelengths and locations of spots depend on how large area is illuminated, it would be extremely difficult to reproduce such a dynamic pattern using standard materials and techniques. A read-out device would essentially work along the process in Fig. 1, analysing the large-scale pattern while illuminating a central area, with a stepwise increased beam radius. In addition it would check for the correct circular polarisation. For further security a colloidal crystal with defects could be realised, i.e. droplets/beads of non-cholesteric material or with different size or pitch would be introduced. Each defect will not only appear different from other droplets, but the fact that it cannot participate in inter-droplet photonic communication means that it will leave a mark in the spot pattern in the surrounding droplets. Thus, it would be easy to generate a pattern that is absolutely unique and almost impossible to fake.

In summary, we have demonstrated and explained the unique optical properties of monodisperse cholesteric liquid crystal droplets, in particular when arranged in a hexagonally close-packed colloidal crystal. Multiple six-fold symmetric patterns of coloured spots arise, reflecting photonic communication between droplets, directly or mediated via a total internal reflection event at the surface of the continuous phase. Strong wavelength selectivity is provided by the cholesteric helix and its consequent photonic crystal character. The same behaviour applies also to cholesteric shells with radial helix orientation, since the optics relevant for the described behaviour is identical for droplets and shells. This may give further means of adding responsiveness and tuneability. To illustrate the potential for applications of these systems we have outlined four device categories that could be realised based on their unique dynamic optical patterns: a combined all-optical switch, monochromator and retroreflector; an in-plane omnidirectional beam coupler; autonomous sensors; and high-security identification tags.

Acknowledgements

Financial support from the National Research Foundation (Korea), grant number 490-20110016, is gratefully acknowledged.

References

1 J. P. F. Lagerwall and G. Scalia, *Curr. Appl. Phys.*, 2012, **12**, 1387–1412.
2 M. ONeill and S. Kelly, *Adv. Mater.*, 2011, **23**, 566–584.
3 N. Y. Ha, S. M. Jeong, S. Nishimura and H. Takezoe, *Adv. Mater.*, 2010, **22**, 1617.
4 N. Ha, Y. Ohtsuka, S. Jeong, S. Nishimura, G. Suzaki, Y. Takanishi, K. Ishikawa and H. Takezoe, *Nat. Mater.*, 2008, **7**, 43–47.
5 E. Enz, V. La Ferrara and G. Scalia, *ACS Nano*, 2013, **7**, 6627–6635.
6 J. D. Davies, Dylan, R. Vaccaro, Antonio, M. Morris, Stephen, N. Herzer, P. H. J. Schenning, Albertus and W. M. Bastiaansen, Cees, *Adv. Funct. Mater.*, 2013, **23**, 2723–2727.
7 N. Herzer, H. Guneysu, J. D. Davies, Dylan, D. Yildirim, R. Vaccaro, Antonio, J. Broer, Dirk, W. M. Bastiaansen, Cees and P. H. J. Schenning, Albertus, *J. Am. Chem. Soc.*, 2012, **134**, 7608–7611.
8 A. Munoz, M. E. McConney, T. Kosa, P. Luchette, L. Sukhomlinova, T. J. White, T. J. Bunning and B. Taheri, *Opt. Lett.*, 2012, **37**, 2904–2906.
9 M. Humar and I. Musevic, *Opt. Express*, 2010, **18**, 26995–27003.
10 B. Park, M. Kim, S. W. Kim, W. Jang, H. Takezoe, Y. Kim, E. H. Choi, Y. H. Seo, G. S. Cho and S. O. Kong, *Adv. Mater.*, 2009, **21**, 771.
11 M. Moreira, I. Carvalho, W. Cao, C. Bailey, B. Taheri and P. Palffy-Muhoray, *Appl. Phys. Lett.*, 2004, **85**, 2691–2693.
12 Y. Han, K. Pacheco, C. W. M. Bastiaansen, D. J. Broer and R. P. Sijbesma, *J. Am. Chem. Soc.*, 2010, **132**, 2961–2967.
13 H. Liang, J. Noh, R. Zentel, P. Rudquist and J. Lagerwall, *Philos. Transact. A Math. Phys. Eng. Sci.*, 2013, **371**, 20120258.
14 H.-L. Liang, S. Schymura, P. Rudquist and J. Lagerwall, *Phys. Rev. Lett.*, 2011, **106**, 247801.
15 T. Lopez-Leon, A. Fernandez-Nieves, M. Nobili and C. Blanc, *Phys. Rev. Lett.*, 2011, **106**, 247802.
16 T. Lopez-Leon, V. Koning, K. B. S. Devaiah, V. Vitelli and A. Fernandez-Nieves, *Nat. Phys.*, 2011, **7**, 391–394.
17 M. A. Gharbi, D. Sec, T. Lopez-Leon, M. Nobili, M. Ravnik, S. Zumer and C. Blanc, *Soft Matter*, 2013, **9**, 6911–6920.
18 V. Koning, T. Lopez-Leon, A. Fernandez-Nieves and V. Vitelli, *Soft Matter*, 2013, **9**, 4993–5003.
19 Y. Geng, D. Sec, L. Almeida, Pedro, D. Lavrentovich, Oleg, S. Zumer and H. Godinho, Maria, *Soft Matter*, 2013, **9**, 7928–7933.
20 D. Sec, T. Lopez-Leon, M. Nobili, C. Blanc, A. Fernandez-Nieves, M. Ravnik and S. Zumer, *Phys. Rev. E*, 2012, **86**, 020705(R).
21 T. Lopez-Leon and A. Fernandez-Nieves, *Colloid Polym. Sci.*, 2011, **289**, 345–359.
22 D. R. Nelson, *Nano. Lett.*, 2002, **2**, 1125–1129.
23 E.-K. Fleischmann, H.-L. Liang, N. Kapernaum, F. Giesselmann, J. P. F. Lagerwall and R. Zentel, *Nat. Commun.*, 2012, **3**, DOI: 10.1038/ncomms2193.
24 Y. Uchida, Y. Takanishi and J. Yamamoto, *Adv. Mater.*, 2013, **25**, 3234–3237.
25 D. Liu, W. M. Bastiaansen, Cees, M. J. den Toonder, Jaap and J. Broer, Dirk, *Angew. Chem. (Int. Ed.)*, 2012, **51**, 892–896.
26 S. Chae, H. Min, J. Lee, B. Hwang, W. Sung, W. Jang, Y. Yoo, J. Oh, J. Park, D. Kang, D. Kim, Y. Kim and H. Baik, *Adv. Mater.*, 2013, **25**, 1408–1414.
27 Y. Yang, M. Suzuki, S. Owa, H. Shirai and K. Hanabusa, *J. Mater. Chem.*, 2006, **16**, 1644–1650.